

16 **Abstract**

17 The current strategies to eradicate bacteria require that the antimicrobial agent either penetrate
18 or disrupt the bacterial membrane. In *Escherichia coli* (*E.coli*) as a model of Gram negative
19 strains, the antimicrobials have to cross two barriers - the outer and the inner membrane being
20 the latter composed by ~ 77 % phosphatidylethanolamine (PE), ~ 13 % phosphatidylglycerol
21 (PG) and ~ 10 % cardiolipin (CL) lipids. Each one of these lipid families shares the same
22 headgroup, but contains acyl chains with varying length and degree of unsaturation. Bacteria
23 adapt their membrane lipid composition and metabolism in response to environmental signals,
24 such as the temperature, resulting in different interactions with exogenous molecules, e.g.
25 antibacterial agents. Herein, bacterial model membranes are prepared to evaluate the lipid-lipid
26 interactions in Langmuir monolayers of binary mixtures at several molar ratios of PE and PG
27 or CL at human physiological temperature (37°C). Both PE:PG and PE:CL monolayers were
28 stable at 37 °C and presented higher molecular areas ($> 20 \text{ \AA}^2 \cdot \text{molecule}^{-1}$) than at 23 °C.
29 However, these lipid mixtures presented liquid-expanded state and rigidity (inverse of the
30 compressibility modulus $\sim 90 \text{ mN} \cdot \text{m}^{-1}$) slightly lower than at 23°C. Such athermality at
31 biologically relevant temperatures may favour the preservation of the biological functions of
32 *E.coli*.

33

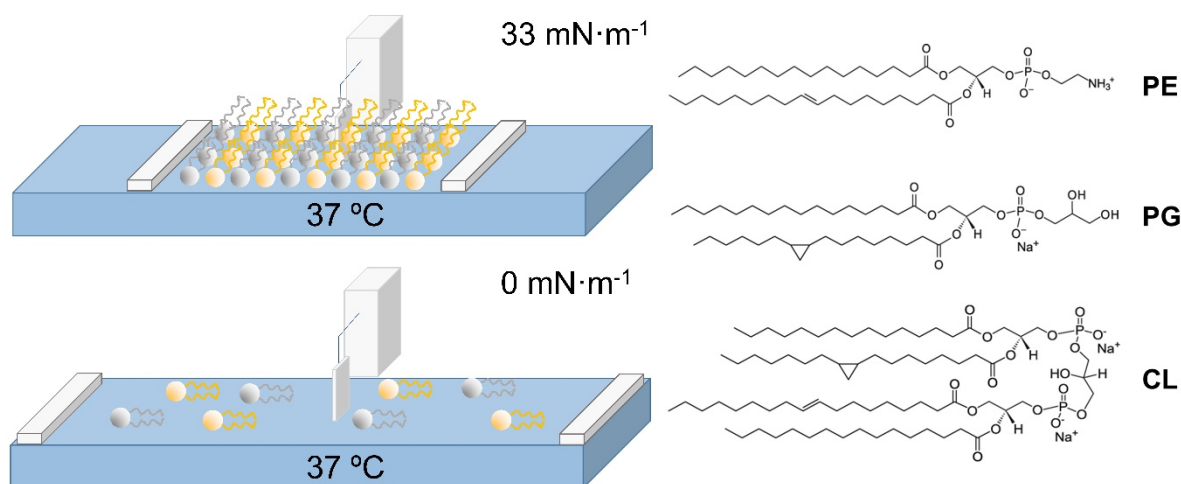
34

35 **1 Introduction**

36 Most recent strategies to eradicate bacteria, rely on disruption of the bacterial membrane with
37 nano-formulated antimicrobial agents that ultimately causes cell death with less probability for
38 resistance development (Ivanova et al. 2017; Ferreres et al. 2018; Hoyo et al. 2019a). However,
39 the majority of clinically relevant antibiotics need to cross the membrane of Gram-negative
40 bacteria such as *Escherichia coli* (*E.coli*) in order to exert their antibacterial effect. The outer
41 membrane of *E.coli* is mainly composed of lipopolysaccharides, while the inner membrane
42 contains mainly lipids (~ 77 % phosphatidylethanolamine (PE), ~ 13 % phosphatidylglycerol
43 (PG), and ~ 10 % cardiolipin (CL)) and proteins (Shokri and Larsson 2004; Yeagle 2016).
44 Langmuir and Langmuir Blodgett (LB) films have been used to study *in vitro* the antibacterial
45 mechanism of new agents (Fernandes et al. 2017; Ivanova et al. 2018). Simple and reproducible
46 mammalian (Nichols-Smith et al. 2004; Domènech et al. 2006), thylakoid (Hoyo et al. 2012;
47 Hoyo et al. 2015; Hoyo et al. 2016a; Hoyo et al. 2016b), and bacterial (Gidalevitz et al. 2003;
48 Clausell et al. 2007; López-Montero et al. 2008; López-Montero et al. 2010; Michel et al. 2015;
49 Michel et al. 2017) membrane models have been prepared using these techniques for studying
50 the interactions of exogenous molecules, including antibacterial agents, with bacterial
51 membranes. Previous works reported the application of inner bacterial membrane models
52 composed of a single lipid, e.g. dipalmitoylphosphatidylglycerol (DPPG) (Gidalevitz et al.
53 2003) and palmitoyloleoylphosphatidylglycerol (POPG) (Gidalevitz et al. 2003; Clausell et al.
54 2007), while the outer bacterial membrane was mimicked by lipopolysaccharides (LPS)
55 (Clausell et al. 2007). The validity of these models was compromised by the use of only one
56 lipid and the absence of PE, the major lipid present in bacterial inner membranes (Yeagle 2016).
57 Michel et al. (Michel et al. 2015) mimicked separately the outer and inner leaflets by the use of
58 LPS and a ternary mixture of monounsaturated bacterial phospholipids. Furthermore, the same
59 authors prepared a similar model with a unique structure combining the LB and Langmuir

60 Schaefer techniques (Michel et al. 2017). Both models lacked the use of natural lipid
61 constituents of the bacterial membranes. López-Montero *et al.* (López-Montero et al. 2008;
62 López-Montero et al. 2010) solved this drawback using an *E. coli* polar lipid extract (PLE)
63 comprised of a myriad of lipid structures sharing the same headgroup. Recently, we prepared
64 biomimetic membrane models using also a myriad of lipid structures to evaluate the lipid-lipid
65 interactions in binary mixtures composed of PE and PG or CL at 23 °C. The models revealed
66 that all tested ratios of lipids were in fluid state (liquid expanded -LE-) and minor changes in
67 terms of membrane rigidity were observed among the PE content in the mixture (Hoyo et al.
68 2019b).

69 Bacteria regulate their metabolism, membrane lipid composition and the degree of unsaturation
70 of their hydrocarbon chains as a response to environmental signals (Larsson and Törnkvist
71 1996; Shokri and Larsson 2004). Several biomimetic membrane studies have shown relevant
72 differences in the lipid-lipid (Suárez-Germà et al. 2011) or lipid-polymer (Krajewska et al.
73 2013a; Krajewska et al. 2013b) interactions upon increasing the temperature. Therefore,
74 studying the role of temperature in bacterial mimetic inner membranes could anticipate the
75 interactions between novel antibacterial agents and the membrane. Herein, our previous study
76 of PE:PG and PE:CL monolayers at 23 °C (Hoyo et al. 2019b) is reproduced at human
77 physiological temperature of 37 °C. The surface pressure-area isotherms of Langmuir films
78 describe the physical states, rigidity and thermodynamic properties of the monolayers at the
79 air/water interface (Scheme 1). The use of natural *E. coli* lipid extracts of the myriad of
80 structures corresponding to each lipid, and the study of several binary mixtures of lipids,
81 including the biologically relevant one, allows for a reliable evaluation of the lipid-lipid
82 interactions in *E. coli* mimetic membranes to serve potentially as a model for validation of novel
83 antibacterial agents.



84
 85 **Scheme 1.** Langmuir monolayer formation and representative chemical structure of the myriad
 86 of lipid structures that shares the same headgroup: phosphatidylethanolamine (PE),
 87 phosphatidylglycerol (PG) and cardiolipin (CL) in lipid extracts from *E. coli* (see section 2.1).

88
 89 **2 Materials and methods**

90 *2.1 Materials*

91 Avanti Polar Lipids provided PE (# 840027), PG (# 841188) and CL (# 841199) extracted from
 92 *E. coli*. Each lipid represents a myriad of structures that share the same headgroup, but differ in
 93 their degree and position of unsaturation. CHCl_3 and phosphate buffer solution (PBS) tablets
 94 were provided by Sigma-Aldrich (Spain). Ultrapure MilliQ water with a resistivity of $18.2 \text{ M}\Omega$
 95 $\cdot \text{cm}^{-1}$ was used in cleaning procedures and for PBS at pH 7.4 preparation.

96
 97 *2.2 Surface pressure – area isotherms*

98 PE, PG, and CL solutions in CHCl_3 ($0.5 \text{ mg}\cdot\text{mL}^{-1}$) and the corresponding mixtures at different
 99 molar ratios were prepared by mixing each stock solution and were stored at $-20\text{ }^\circ\text{C}$ until used.
 100 Surface pressure – area (π -A) isotherms were performed in a Langmuir trough equipped with

101 two mobile barriers (KSV NIMA, model KN2002, Finland) with a total area of 273 cm²
102 mounted on an antivibration table and housed in an insulation box at 37 ± 1 °C. The temperature
103 was maintained by connecting a thermostatic water bath to the inner circuit of the Langmuir
104 trough and placing a temperature probe in the subphase. The Langmuir trough was cleaned with
105 CHCl₃ and water. After subphase addition, the surface was further cleaned by suctioning.
106 Immediately, 25 μL of the lipid or lipid mixture solution was added dropwise into the trough,
107 and after 10 minutes evaporation of CHCl₃, the barriers were compressed at 25 cm²·min⁻¹. $\pi -$
108 A isotherms were performed by triplicate.

109

110 *2.3 Data analysis*

111 *Physical states*

112 The inverse of the compressibility modulus (C_s^{-1}) was obtained from the π -A isotherms
113 calculated according to Equation 1, where A is the mean area per molecule (Å²·molecule⁻¹), π
114 the surface pressure (mN·m⁻¹) and T the absolute temperature (K).

$$115 \quad C_s^{-1} = -A \left(\frac{d\pi}{dA} \right)_T \quad \text{Equation 1}$$

116

117 *Thermodynamic study*

118 The mixing energy (ΔG_{mix}) of a mixture is obtained from the following equation in which A^E
119 represents the excess area, A_1 and A_2 the area per molecule for the individual components, A_{12}
120 the mean area per molecule for the mixture, x_1 and x_2 the molar fraction for each component,
121 G^E the excess free energy of mixing, N_A the Avogadro's number, R the gas constant and T the
122 absolute temperature.

123

124
$$A^E = A_{12} - (x_1 A_1 + x_2 A_2)$$
 Equation 2

125
$$G^E = N_A \int_0^\pi A^E d\pi$$
 Equation 3

126
$$\Delta G_{\text{mix}} = \Delta G_{\text{id}} + G^E$$
 Equation 4

127
$$\Delta G_{\text{id}} = RT (x_1 \ln x_1 + x_2 \ln x_2)$$
 Equation 5

128

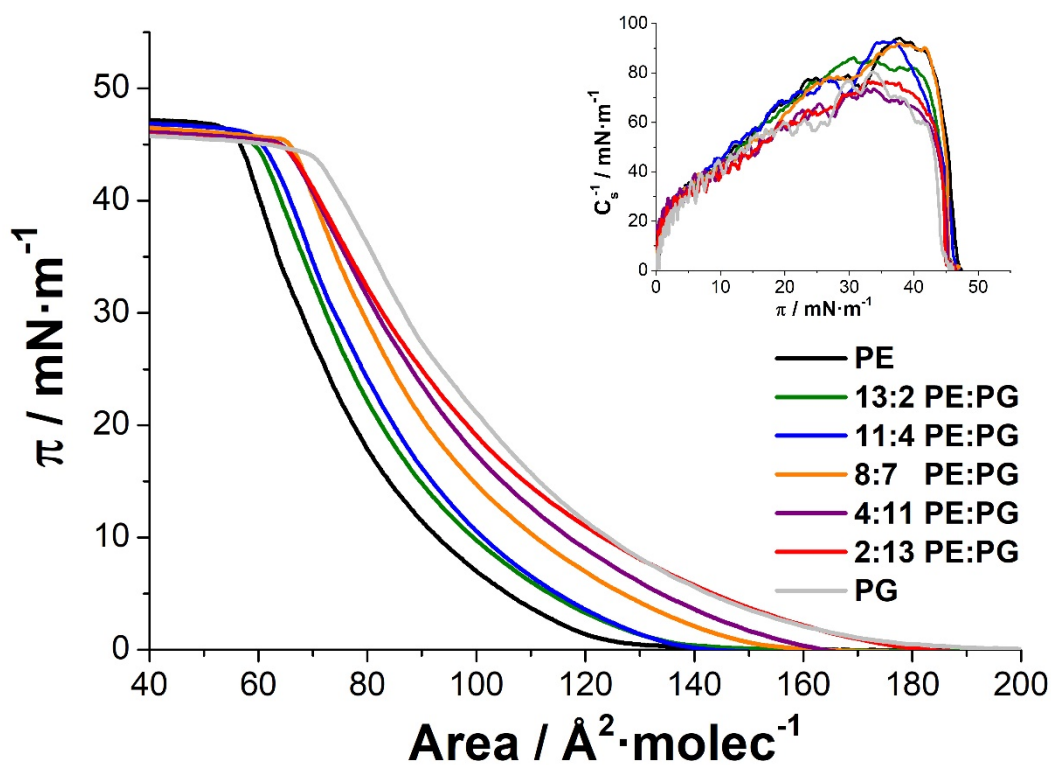
129

130 **3. Results**

131 *3.1 π -A isotherms, physical states and mixing behaviour of PE:PG system*

132 The lift-off area for PE and PG at 37 °C was observed at 135 and 185 Å²·molecule⁻¹ and the
133 collapse at $\pi = 46$ and 45 mN·m⁻¹, respectively (fig. 1). The isotherms were continuous and the
134 C_s^{-1} curves reached their maximum ($C_s^{-1}_{max}$) at ≈ 94 and 80 mN·m⁻¹ (inset of fig. 1) for PE
135 and PG respectively, confirming the LE (Vitovič et al. 2006) physical state of the system. The
136 studied PE:PG mixtures show similar isotherms and C_s^{-1} curves, mainly differing in the lift-off
137 area that was higher upon increasing the amount of PG in the mixture. PE and PG showed
138 similar size and shape. However, the PG headgroup is slightly larger than the headgroup of PE,
139 explaining the differences observed in the lift-off area. The average molecular area (fig. 2A)
140 showed slight random deviations from the additivity rule (dashed line), confirming the ideal
141 behaviour of the PE:PG Langmuir films regardless the PG content. The ΔG_{mix} curves (fig. 2B)
142 presented negative values for all tested mixtures, confirming their stability (Roche et al. 2006).

143



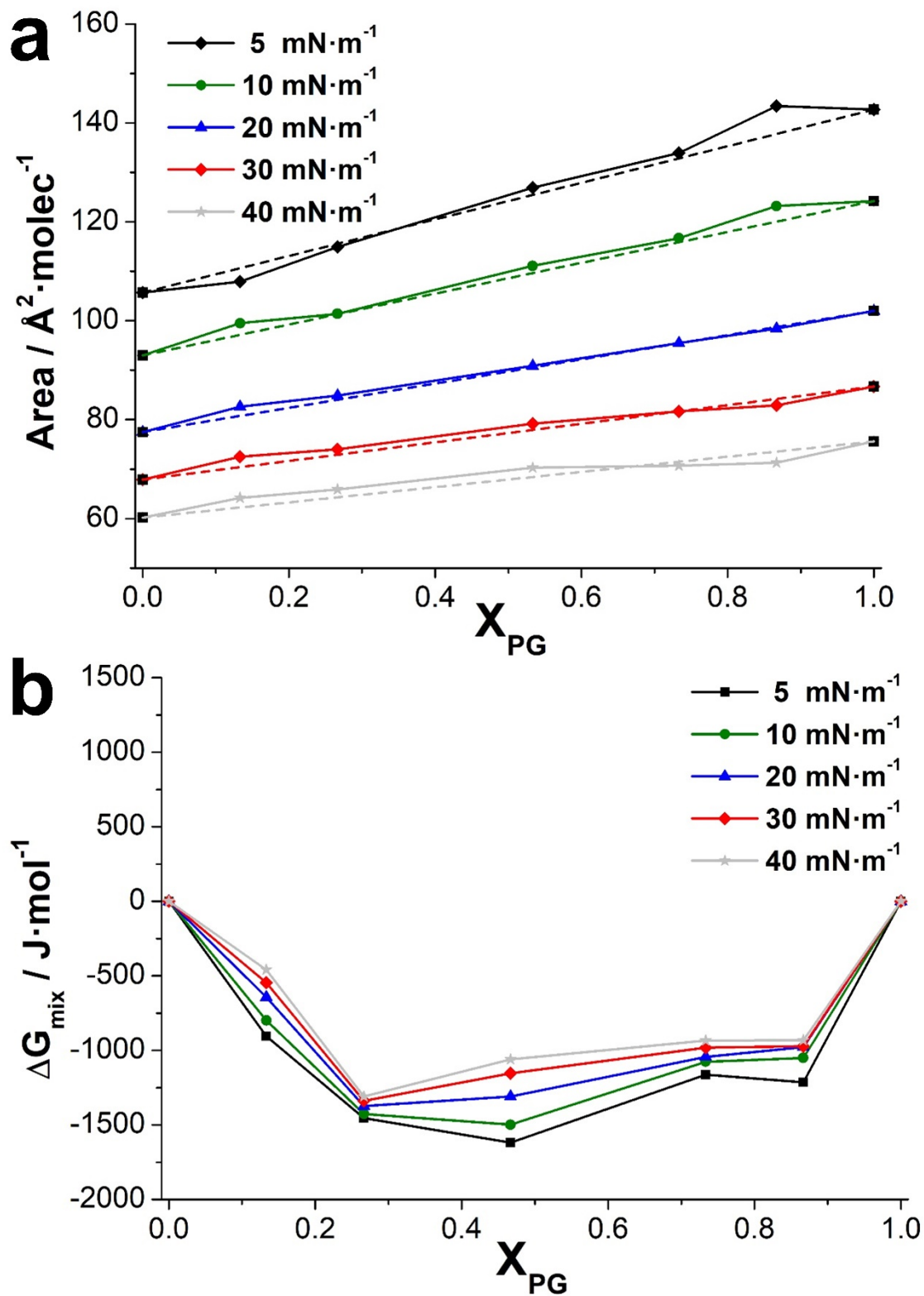
144
 145 **Fig. 1** π -A isotherms for PE, PG and PE:PG mixtures on PBS subphase at 37 °C. Inset: Inverse
 146 of the compressibility modulus *vs.* surface pressure corresponding to the described π -A
 147 isotherms.

148

149 3.2 π -A isotherms, physical states and mixing behaviour of PE:CL system

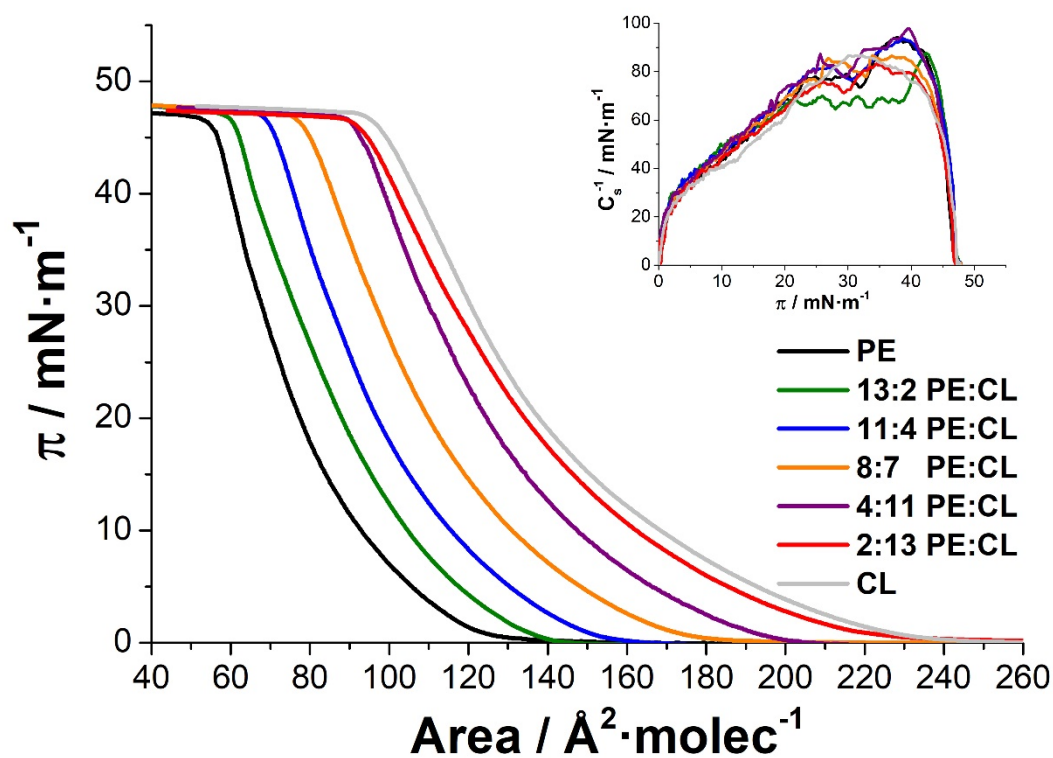
150 The CL π -A isotherm at 37 °C (fig. 3) showed the lift-off area at 240 Å²·molecule⁻¹ and the
 151 collapse of the film at $\pi = 47$ mN·m⁻¹. The $C_s^{-1}{}_{max} \approx 94$ mN·m⁻¹ (inset of fig. 3) indicates the
 152 LE physical state of the monolayer (Vitovič et al. 2006). The comparable hydrocarbon chains
 153 of PE and CL lead to similar isotherms and C_s^{-1} curves for their mixed monolayers. The
 154 increased molecular area observed upon increasing the CL content is correlated with the larger
 155 volume that occupy the four hydrocarbon chains in CL compared to the volume of two
 156 hydrocarbon chains in PE (Baumgärtner et al. 2007; Boyd et al. 2017).

157



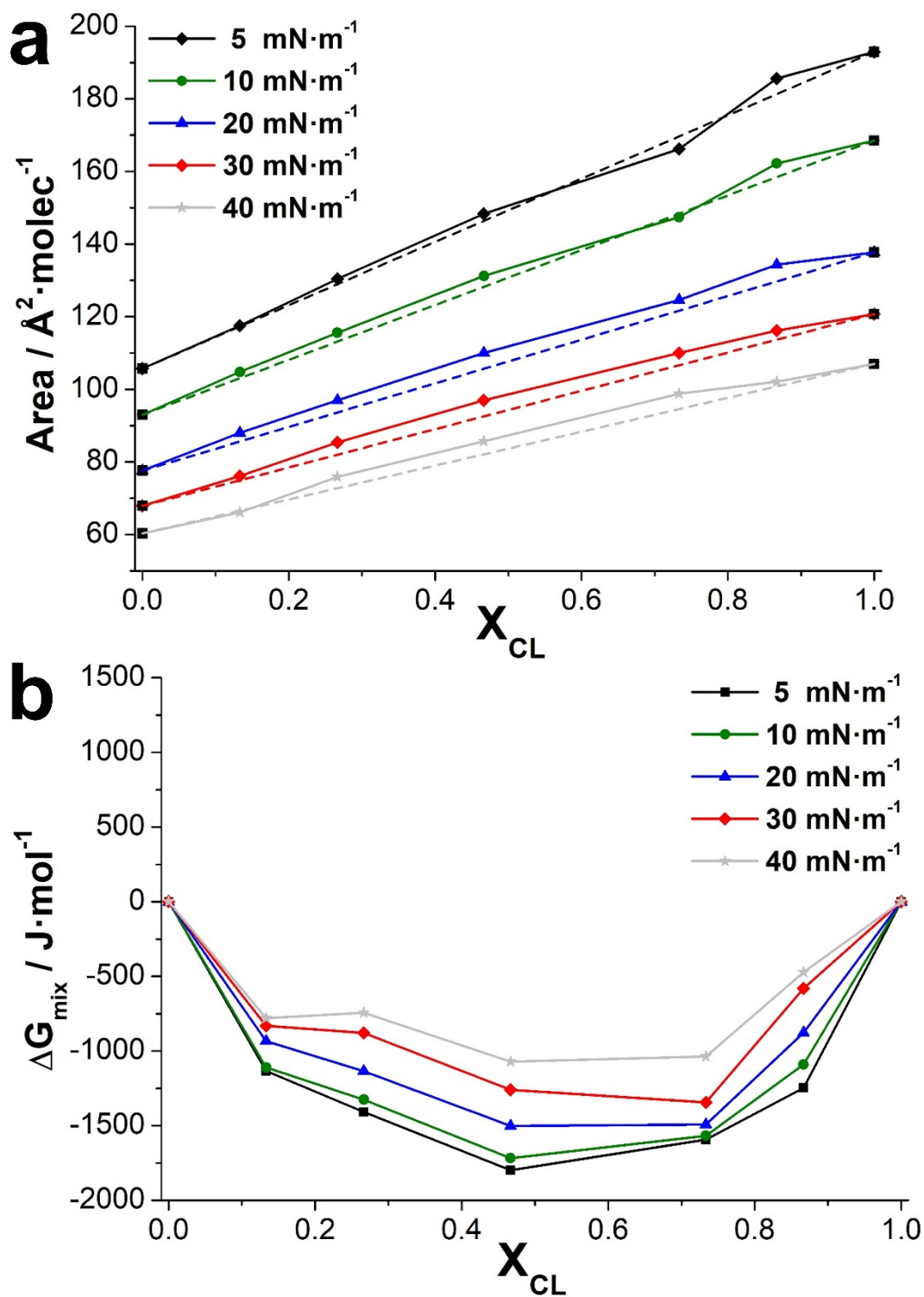
158

159 **Fig. 2** a) Mean area per molecule vs. molar fraction and b) mixing energy vs. molar fraction at
 160 several surface pressures for the PE:PG system at 37 °C. The discontinuous straight line
 161 represents the ideal behaviour for each surface pressure.



162
 163 **Fig. 3** π -A isotherms for PE, CL and PE:CL mixtures on PBS subphase at 37 °C. Inset: Inverse
 164 of the compressibility modulus *vs.* surface pressure corresponding to the described π -A
 165 isotherms.

166
 167 The mean area per molecule *vs.* molar fraction curves (fig. 4A) exhibited slightly positive
 168 deviations from the additivity rule (dashed line), corroborating that PE:CL system constitutes
 169 slightly non-ideal films at $\pi > 5 \text{ mN}\cdot\text{m}^{-1}$. The negative ΔG_{mix} values (fig. 4B) observed for all
 170 the mixtures indicate the stability (Roche et al. 2006) of the studied PE:CL mixtures.



171

172 **Fig. 4** a) Mean area per molecule vs. molar fraction and b) mixing energy vs. molar fraction at
 173 several surface pressures for the PE:CL system at 37°C. The discontinuous straight line
 174 represents the ideal behaviour for each surface pressure.

175 4. Discussion

176 The current work used a myriad of natural lipid structures that share the same headgroup, but
177 contain acyl chains with different length and degree of unsaturation, for preparing model
178 bacterial membranes. PE:PG and PE:CL mixtures at 37 °C showed higher lift-off areas (fig. 1
179 and fig. 3) than those observed at 23 °C (Hoyo et al. 2019b). On the contrary, the collapse
180 surface pressure was lowered upon the increase of temperature. Higher temperature favours the
181 lipid vibrations and the dissociation of ionisable groups (Krajewska et al. 2013b) -PG and CL
182 headgroups - inducing higher molecular areas. The PE:PG system yielded a higher lift-off area
183 difference $\sim 30 \text{ \AA}^2 \cdot \text{molecule}^{-1}$ than PE:CL $\sim 20 \text{ \AA}^2 \cdot \text{molecule}^{-1}$ upon the temperature increase,
184 attributed to the stronger interactions observed in the PE:PG system compared to PE:CL at 23
185 °C (Hoyo et al. 2019b). Similarly, Suárez-Germà et al. (Suárez-Germà et al. 2011) observed
186 that monolayers of lipids with PE headgroup presented higher lift-off area as the number of
187 unsaturations of the hydrocarbon chains or the temperature was increased, according to
188 observations for DPPG (Krajewska et al. 2013b) and dipalmitoylphosphatidylcholine
189 (Krajewska et al. 2013a). The characteristics of the acyl chains (unsaturation and chains length)
190 contributed to the steric hindrances between individual lipids resulting in a lower packing.

191 The $C_s^{-1}_{max}$ for the single lipids and their corresponding mixtures decreased below $100 \text{ mN} \cdot \text{m}^{-1}$
192 ¹, indicating that all studied systems present LE physical state in accordance to the results
193 observed at 23°C (Hoyo et al. 2019b), where only PE lipid monolayer reached the liquid
194 condensed (LC) state. The increase of the temperature favours the dissociation of ionisable
195 groups (Krajewska et al. 2013b) and lowers the packing, thus yielding fluid phases. The rigidity
196 of the studied systems at 23 °C was slightly higher than at 37° C. The characteristics of the
197 isotherms and the LE state observed for the binary PE:PG and PE:CL systems (fig. 1 and 3) are
198 in line with previous studies using a natural ternary mixture (Clausell et al. 2004; López-

199 Montero et al. 2008). The presence of unsaturations promoted the formation of fluid phases in
200 our PE:PG and PE:CL systems (inset of fig. 1 and 3). Such phenomenon was also described
201 (Suárez-Germà et al. 2011) for palmitoyloleoylphosphatidylethanolamine (POPE) and POPG
202 that became less rigid upon increasing the number of unsaturations whereas the saturated
203 dipalmitoylphosphatidylethanolamine reached solid state (S) (Hernández-Borrell and
204 Domènech 2017). The PE:PG and PE:CL systems formed almost ideal monolayers at 37 °C
205 (fig. 2A and 4A). In contrast, the PE:CL system showed non-ideal films at 23 °C, inducing non-
206 favoured mixtures when the amount of PE or CL was above 20 % and $\pi \geq 30 \text{ mN}\cdot\text{m}^{-1}$ (Hoyo et
207 al. 2019b). This observation is explained by the higher repulsion and vibration between lipids
208 upon increasing the temperature.

209 The thermodynamic study showed negative ΔG_{mix} values for all studied systems (fig. 2B and
210 4B), thus indicating the stability of the mixtures and the absence of phase separation (Gzyl-
211 Malcher et al. 2008) domains for both PE:PG and PE:CL systems, regardless the PE:lipid ratio,
212 contrarily to the PE:CL system unstable at 23 °C. The formation of domains was observed for
213 the POPE:CL (Domènech et al. 2006) and POPE:POPG 3:1 (Seeger et al. 2009; Picas et al.
214 2010; Suárez-Germà et al. 2011) systems both in LB and supported planar bilayers - widely
215 used for biomimetic membranes construction (Domènech et al. 2006; Hoyo et al. 2013) - below
216 and above the melting temperature. These observations were attributed to the tendency of POPE
217 to form LC phase (Suárez-Germà et al. 2011) and the presence of Ca^{2+} ions that resulted in
218 stronger interaction with POPG than with POPE (Picas et al. 2010), thus inducing phase
219 separation. Oppositely to the POPE:POPG and POPE:CL systems, the thermodynamic studies
220 of biomimetic membranes with a natural myriad of bacterial lipids indicated the absence of
221 phase separation domains at 37 °C (López-Montero et al. 2008). Nevertheless, the same authors
222 (López-Montero et al. 2008) observed their presence by epifluorescence microscopy, whereas
223 Domènech et al. (Domènech et al. 2006) did not detect such domains by atomic force

224 microscopy (AFM), in line with our thermodynamic results (fig. 2B and fig. 4B). Most
225 probably, the use of selective fluorescent dyes favors the visualization of such domains in
226 biomimetic membranes (López-Montero et al. 2008), as previously observed in natural bacterial
227 membranes (Mileykovskaya et al. 2001). These apparently contradictory results with some
228 previous studies may be explained by the limitations of the thermodynamic study applied to a
229 multicomponent system. Despite the fact that we have studied binary PE:PG and PE:CL
230 systems at several molar ratios, each lipid named by its headgroup contains several structures,
231 corresponding to different chain length and unsaturation, building a multicomponent system.
232 Therefore the emergence of nanoscale lipid domains could be possible as observed in biological
233 membranes (Jacobson et al. 2007).

234 The temperature of the bacterial membrane environment is an important parameter, since some
235 of the lipid constituents of these membranes present phase transition close to the physiological
236 human temperature (Silvius 1982). Therefore, the physical state influences both the
237 permeability of the membrane and the interactions of the lipids with other membrane
238 components, altering consequently their function (Barrera et al. 2012). Several mechanisms
239 have been reported by which antibacterial agents target bacteria and alter their membrane
240 properties (Epanand et al. 2016). Therefore, the physical state and the fluidity of the bacterial
241 membrane is of high relevance for the development of bactericidal agents. Several bacterial
242 model membranes with different degree of similarity to the real membranes are described in
243 the literature, but most of them are composed by only one or two lipid structures. Despite that
244 some of these studies used unsaturated lipids to enhance the fluidity of the resulting membranes,
245 the effect of the biological myriad of lipid structures was not evaluated, thus the reduction of
246 fluidity was not considered neither the different interaction of the lipid structures with the
247 antibacterial agent. In our work, the fluidity of the model membrane formed at 37 °C was
248 compared to the fluidity of a membrane formed at 23 °C, concluding the athermalicity of the

249 rigidity and physical state for PE:PG and PE:CL systems at biologically relevant temperatures.
250 These results correlate with previous reports for other lipid systems at LE state (López-Montero
251 et al. 2008) and may explain the ability of *E.coli* membranes to maintain their functionality
252 across a broad temperature range (Remaut and Fronzes 2014) due to intermolecular hydrogen
253 bonding between lipids and transmembrane proteins allowing the correct protein insertion and
254 function in the membrane (Domènech et al. 2006). The observed athermalicity suggested that
255 the effect of antibacterial agents on model lipid membranes would be similar, regardless room
256 or human physiological temperature.

257

258

259 **5. Conclusions**

260 *E.coli* model membranes were prepared using bacterium's natural lipid structures. These
261 biomimetic membranes present almost athermal physical state and rigidity, which may be
262 related to the ability of bacteria to maintain their functions at human physiological temperatures.
263 These observations are of high relevance for the design of novel antimicrobial agents targeting
264 the bacterial membranes. Similar behaviour of the bacterial membrane in the range of 23 to 37
265 °C was detected, despite that the phase transition temperature of some lipid structures present
266 in *E. coli* membranes is close to human physiological temperature. Independently from the
267 different strategies that bacteria adopt to adapt their lipid membrane composition to the
268 temperature of the environment, their bulk membrane behaviour in the studied temperature
269 range was not significantly altered. Novel bactericidal agents targeting the bacterial membrane
270 may be engineered considering the athermalicity of the membrane bulk properties. The simple
271 and reliable bacterial membrane model described in this work may be further used for
272 mechanistic studies in vitro of the interactions between bactericidal agents and bacteria.

273

274 **Acknowledgements**

275 The research leading to these results has received funding from European Community's
276 Horizon 2020 Framework Program H2020 (H2020-720851 project PROTECT - Pre-
277 commercial lines for production of surface nanostructured antimicrobial and anti-biofilm
278 textiles, medical devices and water treatment membranes)

279

280 **Notes**

281 The authors declare no competing financial interest.

282

283 **Author Contributions**

284 The manuscript was written through contributions of all authors. All authors have given
285 approval to the final version of the manuscript.

286

287 *Abbreviations*

288 Cardiolipin from *E. coli* (CL), dipalmitoylphosphatidylglycerol (DPPG), *Escherichia coli*
289 (*E.coli*), *E. coli* polar lipid extract (PLE), Langmuir-Blodgett (LB), liquid condensed (LC),
290 liquid expanded (LE), palmitoyloleoylphosphatidylethanolamine (POPE),
291 palmitoyloleoylphosphatidylglycerol (POPG), phosphatidylethanolamine from *E. coli* (PE),
292 phosphatidylglycerol from *E. coli* (PG)

293 **References**

- 294 Barrera FN, Fendos J, Engelman DM (2012) Membrane physical properties influence
295 transmembrane helix formation. *Proc Natl Acad Sci U S A* 109:14422–14427 . doi:
296 10.1073/pnas.1212665109
- 297 Baumgärtner P, Geiger M, Zieseniss S, Malleier J, Huntington JA, Hochrainer K, Bielek E,
298 Stoeckelhuber M, Lauber K, Scherfeld D, Schwille P, Wäldele K, Beyer K, Engelmann
299 B (2007) Phosphatidylethanolamine critically supports internalization of cell-penetrating
300 protein C inhibitor. *J Cell Biol* 179:793–804 . doi: 10.1083/jcb.200707165
- 301 Boyd KJ, Alder NN, May ER (2017) Buckling under Pressure: Curvature-Based Lipid
302 Segregation and Stability Modulation in Cardiolipin-Containing Bilayers. *Langmuir*
303 33:6937–6946 . doi: 10.1021/acs.langmuir.7b01185
- 304 Clausell A, Busquets MA, Pujol M, Alsina A, Cajal Y (2004) Polymyxin B-lipid interactions
305 in Langmuir-Blodgett monolayers of Escherichia coli lipids: A thermodynamic and
306 atomic force microscopy study. *Biopolymers* 75:480–490 . doi: 10.1002/bip.20165
- 307 Clausell A, Garcia-Subirats M, Pujol M, Busquets MA, Rabanal F, Cajal Y (2007) Gram-
308 negative outer and inner membrane models: Insertion of cyclic cationic lipopeptides. *J*
309 *Phys Chem B* 111:551–563 . doi: 10.1021/jp064757
- 310 Doménech Ò, Merino-Montero S, Montero MT, Hernández-Borrell J (2006) Surface planar
311 bilayers of phospholipids used in protein membrane reconstitution: An atomic force
312 microscopy study. *Colloids Surfaces B Biointerfaces* 47:102–106 . doi:
313 10.1016/j.colsurfb.2005.11.025
- 314 Doménech Ò, Sanz F, Montero MT, Hernández-Borrell J (2006) Thermodynamic and
315 structural study of the main phospholipid components comprising the mitochondrial

316 inner membrane. *Biochim Biophys Acta - Biomembr* 1758:213–221 . doi:
317 10.1016/j.bbamem.2006.02.008

318 Epand RM, Walker C, Epand RF, Magarvey NA (2016) Molecular mechanisms of membrane
319 targeting antibiotics. *Biochim Biophys Acta - Biomembr* 1858:980–987 . doi:
320 10.1016/j.bbamem.2015.10.018

321 Fernandes MM, Ivanova K, Hoyo J, Pérez-Rafael S, Francesko A, Tzanov T (2017)
322 Nanotransformation of vancomycin overcomes the intrinsic resistance of Gram-negative
323 bacteria. *ACS Appl Mater Interfaces* 9:15022–15030 . doi: 10.1021/acsami.7b00217

324 Ferreres G, Bassegoda A, Hoyo J, Torrent-Burgués J, Tzanov T (2018) Metal–Enzyme
325 Nanoaggregates Eradicate Both Gram-Positive and.pdf. *ACS Appl Mater Interfaces*
326 10:40434–40442

327 Gidalevitz D, Ishitsuka Y, Muresan AS, Konovalov O, Waring AJ, Lehrer RI, Lee KYC
328 (2003) Interaction of antimicrobial peptide protegrin with biomembranes. *Proc Natl*
329 *Acad Sci U S A* 100:6302–6307 . doi: 10.1073/pnas.0934731100

330 Gzyl-Malcher B, Filek M, Makyła K, Paluch M (2008) Differences in surface behaviour of
331 galactolipoids originating from different kind of wheat tissue cultivated in vitro. *Chem*
332 *Phys Lipids* 155:24–30 . doi: 10.1016/j.chemphyslip.2008.06.004

333 Hernández-Borrell J, Domènech Ò (2017) Critical Temperature of 1-Palmitoyl-2-oleoyl-sn-
334 glycerol-3-phosphoethanolamine Monolayers and Its Possible Biological Relevance. *J*
335 *Phys Chem B* 121:6882–6889 . doi: <https://doi.org/10.1021/acs.jpcc.7b04021>

336 Hoyo J, Gaus E, Oncins G, Torrent-Burgués J, Sanz F (2013) Incorporation of Ubiquinone
337 in supported lipid bilayers on ITO. *J Phys Chem B* 117:7498–7506 . doi:
338 10.1021/jp4004517

339 Hoyo J, Gaus E, Torrent-Burgués J (2016a) Monogalactosyldiacylglycerol and
340 digalactosyldiacylglycerol role, physical states, applications and biomimetic monolayer
341 films. *Eur Phys J E* 39:1–11 . doi: 10.1140/epje/i2016-16039-0

342 Hoyo J, Gaus E, Torrent-Burgués J (2016b) Influence of membrane galactolipids and surface
343 pressure on plastoquinone behaviour. *Bioelectrochemistry* 111:123–130 . doi:
344 10.1016/j.bioelechem.2016.06.002

345 Hoyo J, Gaus E, Torrent-Burgués J, Sanz F (2015) Biomimetic monolayer films of
346 digalactosyldiacylglycerol incorporating plastoquinone. *Biochim Biophys Acta -*
347 *Biomembr* 1848:1341–1351 . doi: 10.1016/j.bbamem.2015.03.003

348 Hoyo J, Gaus E, Torrent-Burgués J, Sanz F (2012) Electrochemical behaviour of mixed LB
349 films of ubiquinone - DPPC. *J Electroanal Chem* 669:6–13 . doi:
350 10.1016/j.jelechem.2012.01.020

351 Hoyo J, Ivanova K, Gaus E, Tzanov T (2019a) Multifunctional ZnO NPs-chitosan-gallic
352 acid hybrid nanocoating to overcome contact lenses associated conditions and
353 discomfort. *J Colloid Interface Sci* 543:114–121 . doi: 10.1016/j.jcis.2019.02.043

354 Hoyo J, Torrent-Burgués J, Tzanov T (2019b) Physical states and thermodynamic properties
355 of model gram-negative bacterial inner membranes. *Chem Phys Lipids* 218:57–64 . doi:
356 10.1016/j.chemphyslip.2018.12.003

357 Ivanova A, Ivanova K, Hoyo J, Heinze T, Sanchez-Gomez S, Tzanov T (2018) Layer-By-
358 Layer Decorated Nanoparticles with Tunable Antibacterial and Antibiofilm Properties
359 against Both Gram-Positive and Gram-Negative Bacteria. *ACS Appl Mater Interfaces*
360 10:3314–3323 . doi: 10.1021/acsami.7b16508

361 Ivanova K, Ramon E, Hoyo J, Tzanov T (2017) Innovative Approaches for Controlling

362 Clinically Relevant Biofilms: Current Trends and Future Prospects. *Curr Top Med Chem*
363 17:1889–1914 . doi: 10.2174/1568026617666170105143315

364 Jacobson K, Mouritsen OG, Anderson RGW (2007) Lipid rafts: At a crossroad between cell
365 biology and physics. *Nat Cell Biol* 9:7–14 . doi: 10.1038/ncb0107-7

366 Krajewska B, Wydro P, Kyzioł A (2013a) Chitosan as a subphase disturbant of membrane
367 lipid monolayers. The effect of temperature at varying pH: II. DPPC and cholesterol.
368 *Colloids Surfaces A Physicochem Eng Asp* 434:359–364 . doi:
369 10.1016/j.colsurfa.2013.03.015

370 Krajewska B, Wydro P, Kyzioł A (2013b) Chitosan as a subphase disturbant of membrane
371 lipid monolayers. The effect of temperature at varying pH: I. DPPG. *Colloids Surfaces A*
372 *Physicochem Eng Asp* 434:349–358 . doi: 10.1016/j.colsurfa.2013.03.015

373 Larsson G, Törnkvist M (1996) Rapid sampling, cell inactivation and evaluation of low
374 extracellular glucose concentrations during fed-batch cultivation. *J Biotechnol* 49:69–82
375 . doi: 10.1016/0168-1656(96)01534-9

376 López-Montero I, Arriaga LR, Monroy F, Rivas G, Tarazona P, Vélez M (2008) High fluidity
377 and soft elasticity of the inner membrane of *Escherichia coli* revealed by the surface
378 rheology of model langmuir monolayers. *Langmuir* 24:4065–4076 . doi:
379 10.1021/la703350s

380 López-Montero I, Arriaga LR, Rivas G, Vélez M, Monroy F (2010) Lipid domains and
381 mechanical plasticity of *Escherichia coli* lipid monolayers. *Chem Phys Lipids* 163:56–63
382 . doi: 10.1016/j.chemphyslip.2009.10.002

383 Michel JP, Wang Y, Dé E, Fontaine P, Goldmann M, Rosilio V (2015) Charge and
384 aggregation pattern govern the interaction of plasticins with LPS monolayers mimicking

385 the external leaflet of the outer membrane of Gram-negative bacteria. *Biochim Biophys*
386 *Acta - Biomembr* 1848:2967–2979 . doi: 10.1016/j.bbamem.2015.09.005

387 Michel JP, Wang Y, Kiesel I, Gerelli Y, Rosilio V (2017) Disruption of Asymmetric Lipid
388 Bilayer Models Mimicking the Outer Membrane of Gram-Negative Bacteria by an
389 Active Plasticin. *Langmuir* 33:11028–11039 . doi: 10.1021/acs.langmuir.7b02864

390 Mileykovskaya E, Dowhan W, Birke RL, Zheng D, Lutterodt L, Haines TH (2001)
391 Cardiolipin binds nonyl acridine orange by aggregating the dye at exposed hydrophobic
392 domains on bilayer surfaces. *FEBS Lett* 507:187–190 . doi: 10.1016/S0014-
393 5793(01)02948-9

394 Nichols-Smith S, Teh S-YY, Kuhl TL (2004) Thermodynamic and mechanical properties of
395 model mitochondrial membranes. *Biochim Biophys Acta - Biomembr* 1663:82–88 . doi:
396 10.1016/j.bbamem.2004.02.002

397 Picas L, Suárez-Germà C, Teresa Montero M, Hernández-Borrell J (2010) Force spectroscopy
398 study of langmuir-blodgett asymmetric bilayers of phosphatidylethanolamine and
399 phosphatidylglycerol. *J Phys Chem B* 114:3543–3549 . doi: 10.1021/jp910882e

400 Remaut H, Fronzes R (2014) *Bacterial Membranes, Structural and Molecular Biology*. Caister
401 Academic Press

402 Roche Y, Peretti P, Bernard S (2006) Influence of the chain length of ubiquinones on their
403 interaction with DPPC in mixed monolayers. *Biochim Biophys Acta - Biomembr*
404 1758:468–478 . doi: 10.1016/j.bbamem.2006.03.015

405 Seeger H, Marino G, Alessandrini A, Facci P (2009) Effect of Physical Parameters on the
406 Main Phase Transition of Supported Lipid Bilayers. *Biophys J* 97:1067–1076 . doi:
407 10.1016/j.bpj.2009.03.068

408 Shokri A, Larsson G (2004) Characterisation of the Escherichia coli membrane structure and
409 function during fedbatch cultivation. *Microb Cell Fact* 3:9 . doi: 10.1186/1475-2859-3-9

410 Silvius JR (1982) *Thermotropic Phase Transitions of Pure Lipids in Model Membranes and*
411 *Their Modifications by Membrane Proteins*. John Wiley Sons, Inc

412 Suárez-Germà C, Montero MT, Ignés-Mullol J, Hernández-Borrell J, Domènech Ò (2011)
413 Acyl chain differences in phosphatidylethanolamine determine domain formation and
414 LacY distribution in biomimetic model membranes. *J Phys Chem B* 115:12778–12784 .
415 doi: 10.1021/jp206369k

416 Vitovič P, Nikolelis DP, Hianik T (2006) Study of calix[4]resorcinarene-dopamine
417 complexation in mixed phospholipid monolayers formed at the air-water interface.
418 *Biochim Biophys Acta - Biomembr* 1758:1852–1861 . doi:
419 10.1016/j.bbamem.2006.08.011

420 Yeagle PL (2016) *The Membranes of Cells*. Academic Press-Elsevier, San Diego, California
421
422

423 **Figure captions**

424 **Scheme 1.** Langmuir monolayer formation and representative chemical structure of the myriad
425 of lipid structures that shares the same headgroup: phosphatidylethanolamine (PE),
426 phosphatidylglycerol (PG) and cardiolipin (CL) in lipid extracts from *E. coli* (see section 2.1).

427 **Fig. 1** π -A isotherms for PE, PG and PE:PG mixtures on PBS subphase at 37°C. Inset: Inverse
428 of the compressibility modulus *vs.* surface pressure corresponding to the described π -A
429 isotherms.

430 **Fig. 2** a) Mean area per molecule *vs.* molar fraction and b) mixing energy *vs.* molar fraction at
431 several surface pressures for the PE:PG system at 37°C. Discontinuous straight line represents
432 the ideal behaviour for each surface pressure.

433 **Fig. 3** π -A isotherms for PE, CL and PE:CL mixtures on PBS subphase at 37°C. Inset: Inverse
434 of the compressibility modulus *vs.* surface pressure corresponding to the described π -A
435 isotherms.

436 **Fig. 4** a) Mean area per molecule *vs.* molar fraction and b) mixing energy *vs.* molar fraction at
437 several surface pressures for the PE:CL system at 37°C. Discontinuous straight line represents
438 the ideal behaviour for each surface pressure.

439